Available online at www.sciencedirect.com

ScienceDirect

Procedia Engineering 99 (2015) 57 – 66

Procedia Engineering

www.elsevier.com/locate/procedia

"APISAT2014", 2014 Asia-Pacific International Symposium on Aerospace Technology, APISAT2014

Numerical Research on Segmented Flexible Airfoils Considering Fluid-structure Interaction

DONG Hefeng ,WANG Chenxi ,LI Shaobin* ,SONG Xi Zhen

National Key Laboratory on Aero-Engines, School of Energy and Power EngineeringBeihang University.Beijing.100191.China

Abstract

This paper investigated four kinds of segmented flexible airfoils with membrane material on the upper surface and rigid structure on the lower surface. Fluid-structure interaction method was adopted in the numerical simulation for the aerodynamic characteristics and response between flow field and structure of the segmented flexible airfoils. The research focuses on influence of flexible deformation on the lift and drag characteristics and the aerodynamic load distribution of four segmented flexible airfoils at Reynolds number of 1.35×10^5. The results show that the segmented flexible airfoils perform a higher maximum lift coefficient, and effectively delay the stall. At the higher angles of attack, the deformation of the flexible thin membrane could reduce the scale of the separation vortexes. Meanwhile the tiny vortex generated between the flexible segments with the effect called "Fluid Roller Bearing" would impel the separated boundary layer to reattach to the airfoil surface especially on the first half chord region. The three-segment flexible airfoil was proved to be the best airfoil among the four airfoils, which could increase the lift coefficient by 39% near the stall angle of attack compared with its rigid counterpart.

Peer-review under responsibility of Chinese Society of Aeronautics and Astronautics (CSAA)

Keywords: fluid-structure interaction; distribution forms; flexible airfoil; aerodynamic characteristics

* Corresponding author. Tel.: +86-10-82316862
E-mail address: lee_shaobin@buaa.edu.cn

Peer-review under responsibility of Chinese Society of Aeronautics and Astronautics (CSAA)
doi:10.1016/j.proeng.2014.12.508

1. Introduction

Nomenclature

α	Angle of attack
$\overline{C_L}$	Mean lift coefficient
$\overline{C_d}$	Mean drag coefficient
c	Length of the flexible segment
Re	Reynolds number
Π	Elastic parameter
E	Modulus of elasticity
q	Free stream stagnation pressure
t	Thickness of the flexible membrane
U_∞	Free stream velocity
T_u	Turbulence intensity
C_p	Pressure coefficient

Traditional airfoils can perform excellent lift and lift-drag ratio characteristics in a certain range of the angle of attack. But the attached flow will turn to separation at high angles of attack beyond the critical value, which would reduce the lift coefficient dramatically and then enter the stall state. In nature, birds, insects and the other flying creatures are able to adapt variable atmosphere conditions by wing's deformation which may capture and control the fluid around their wings. Inspired by the flying animals, researchers hope to apply the flexible materials to the adaptive deformation airfoils to broaden the range of operating the angle of attack for the airfoils. However, the specific flow mechanisms are still largely unknown. People have done a good deal of investigations in this field which mainly focused on the active and passive control. In terms of active control, Gabor [1, 2] made a better aerodynamic performance of the flexible airfoil through controlling the motion law actively. Chuijie, GuoQiuting et al [3, 4] produced a "Fluid Roller Bearing" effect by giving a suitable traveling wave deformation on the upper surface of the airfoil actively, which inhibits the separation of boundary layer effectively. Curet [5] et al found that using the electrical excitation approach to control the vibration of the flexible wings can improve the lift coefficient significantly in a specific frequency range. On the other hand, in passive control, Lian and Shyy [6, 7] found the coupling interaction of the dynamic effects with the mean curvature of the membrane wing can effectively improve the lift, especially at high angles of attack and delay the occurrence of stall [8]. The research of Albertani, Hu et al [9, 10] revealed that the distribution of flexible structure and materials flexibility have an important impact on the amplitude and frequency of the flexible wings. There is a coupling interaction between the vibration characteristics of flexible wings and the fluctuations of flow field parameters, which is proved by Rojratsirikul [11]. In Shyy's [12] investigation, the airfoil still has a good aerodynamic stability in the case of pulsating inflow.

Compared with the rigid airfoil, the flexible ones have a better aerodynamic performance. For the sake of involving in a coupling of aerodynamic, structure, materials and other subjects, the mechanism for controlling flow of the flexible airfoil is still being researched. This paper using fluid-structure interaction technology researched the lift and drag characteristics of different airfoil types, whose upper surface is segment-flexible membrane structure while the leading and trailing edge maintain rigid. The results reveal that the three-segment flexible airfoil has the best aerodynamic characteristics among the 4 kinds of flexible airfoils, and all the flexible airfoils perform a better performance than the rigid one.

2. Research model

The flexible airfoils used in this paper are based on NACA0012 and their chord length is 0.15m. The upper surface of the flexible airfoils are segmented flexible membrane structure. Four kinds of segmented methods of the flexible airfoils are displayed in Fig 1. Clamped connection mode are used between the flexible segments, and the membrane thickness is 0.4mm. The physical properties of rigid and flexible membrane materials are given in Table 1.

Table 1. Airfoil material properties

Structural forms	Density Kg/m^3	Poisson's ratio	Elastic modulus/MPa
One-segment	1200	0.4	4
Two-segment	1200	0.4	2.5
Three-segment	1200	0.4	2.5
Four-segment	1200	0.4	2.5
Rigid airfoil	7850	0.3	2×10^5

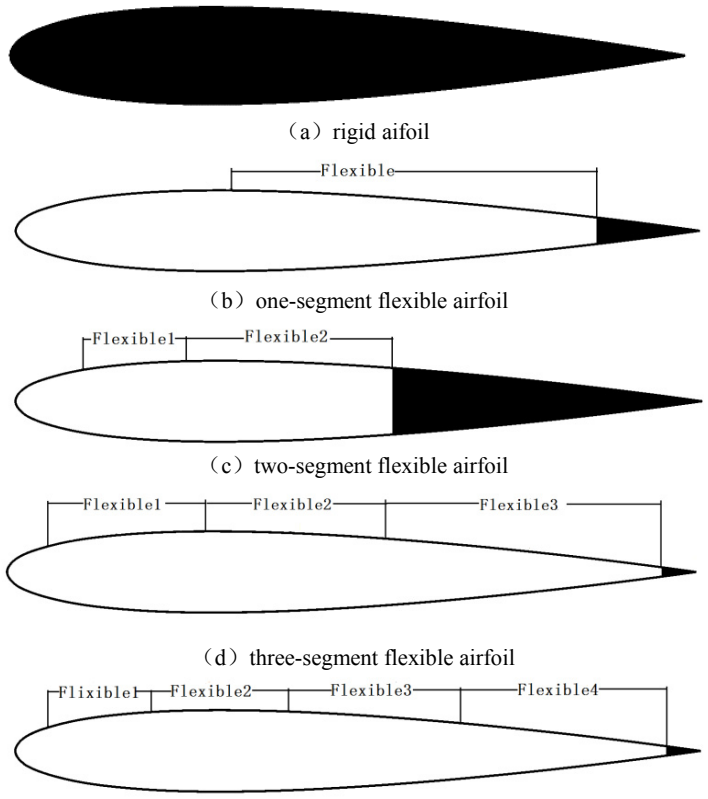

（a）rigid aifoil

（b）one-segment flexible airfoil

（c）two-segment flexible airfoil

（d）three-segment flexible airfoil

（e）four-segment flexible airfoil

Fig. 1. Computational models

3. Numerical Methods and Validation

3.1 Computational domain model

The two-dimensional computational model for the rigid and flexible airfoil is shown in Fig 2. The original point of the domain is the pressure center of airfoil (25% of the chord). The inlet and outlet boundary is 10 and 20 times of chord length, respectively. The distance between the upper and lower boundary is 20 times of the chord length. The computational domain consists three parts, part I part II and part III. Part I represents the solid domain, part II and part III both represent the fluid domain. In order to calculate the characteristics of the angles of attack, the incidences were changed by rotating the computational domains I and II integrally. The computational data and researching parameters were transferred between domains II and III through a circle general interface, whose radius is 5 times of the airfoil chord length.

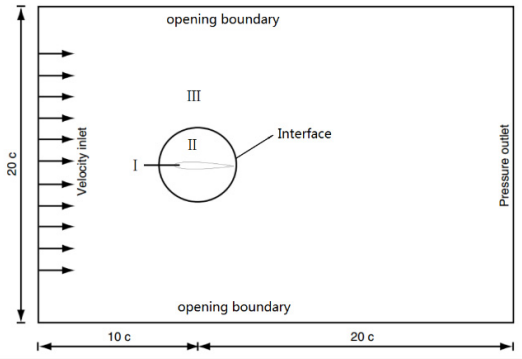

Fig. 2. computational domain

3.2 Grid discretion

The spatial discretization of the computational domain was achieved by ICEM software. Hexahedral element was generated for the solid domain using the swept method. The rigid part used the solid185 element and the SOLSH190 element was used for the flexible part. Both elements are a kind of three-dimensional element defined by eight nodes, each node has three degrees of freedom. They both perform an excellent ability of super-elastic, stress toughened, creep and large deformation and strain. The Solid 185 element is fit for the entity, while the SOLSH190 element is for the membrane structure. In the computational domain Ⅱ, O-type structure grid was used for the region around the surface of the airfoil, and the rest areas adopted unstructured grid. The transition regions near the junction of part Ⅱ and Ⅲ were also unstructured grid, and the other regions of the domain Ⅲ used structural grid. The grid of the entire computational domain and partial view were shown in Fig 3.

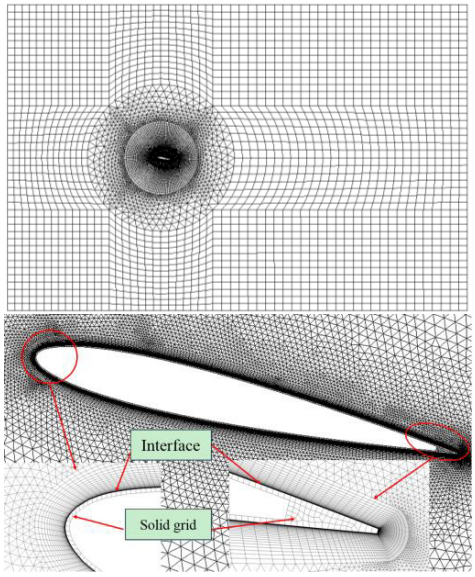

Fig. 3. Computational grid

In the fluid field, there are 400 nodes around the airfoil, and the leading and trailing edge region are concentrated. The distance between the nodes of the first layer and the airfoil surface is 3×10^{-5} chord length, which meets the demand of Y+$\leqslant$1. And the expansion factor along the normal direction of the wall is 1.05, which satisfied the need

of the turbulent and transient model used in the numerical simulation [13]. The number and distribution law of the nodes on both sides of the interface keep consistent so as to reduce the parameter errors during the data transferring. The total number of the nodes is 5×10^4. While in the solid domain, the nodes around the airfoil are distributed uniformly, and the nodes numbers in this part of the 4 kinds of flexible airfoils range from 2400 to 2800.

The grids of computational part I and II are rotated integrally when calculating the incidences characteristics.

3.3 Fluid-structure interaction numerical methods

The interaction between the flexible structure and fluid is a typical fluid-structure interaction issue. The deformation movement of the solid structure changes the flow field around the fluid-structure boundary, while the pressure distribution on the solid surface generated by the fluid also affects the deformation of the solid structure. Due to the coupling of fluid and solid boundary conditions, it is necessary to take the pressure changing in the flow field into consideration when solving the solid equations. In a similar way, the solid deformation must be applied to the solving of the fluid field.

Two-way fluid-structure coupling method was used to solve the fluid and solid field in this research. The fluid field was solved by the finite volume method, while the solid field was calculated with the finite element method. The coupling parameters were iterated through the interface between the fluid and solid field. During the time advancing process, the time iteration in the fluid field, the calculation in the solid field and the data exchanging through the boundary were executed in a time step. It wouldn't finish until the iteration converged. Fig 4 shows the solving flow chart of the fluid-structure interaction for the flexible airfoil. The solving of the fluid field was gained by the CFX solver, and ANSYS transient structural analysis module was used in the flexible structure calculation. The coupling boundaries defined in the MFX (multi-field solver) module made the two-way fluid-structure interaction calculation realizable.

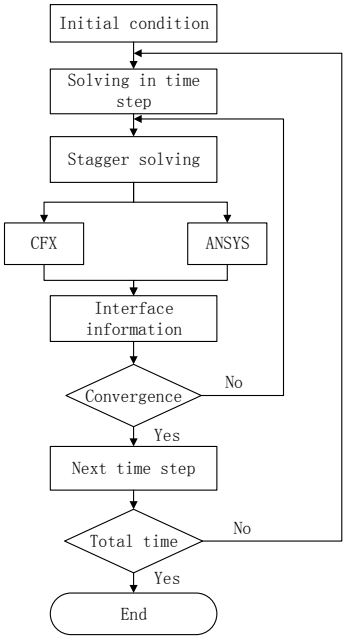

Fig. 4. Fluid-structure interaction flow chart

The γ -θ transition model based on the k-w SST was adopted in the fluid calculation, which was proposed by Menter [14]. This model is designed for predicting the boundary layer transition process. And it has a better ability to capture the transiting phenomenon from laminar flow to turbulent flow, so it can significantly improve the

numerical calculating accuracy.

Under the conditions of the Reynolds number of 1.35×10^5, the computational domain has a horizontal directional inlet velocity of U_∞=14m/s with a turbulence intensity of T_u = 1%. Considering integrally the calculated amount and the calculation precision for the fluid-structure interaction, the physical time step is 0.001 seconds. In order to meet the need of iterative convergence, the aerodynamic and flexible structure parameters change periodically in a small scale, the total calculating time is 2 seconds. The displacement and aerodynamic force were transferred through the fluid-solid interface.

3.4 Numerical method validation

Figure 5 shows the changes of lift and drag coefficient for the rigid airfoil as the angle of attack changed at the Reynolds number of 1.35×10^5. The calculation is in a better agreement with the experimental values [15]. It is obvious that the stall angle of attack given by numerical simulation is slightly smaller than the experimental value, but the calculated differences with the experimental values are acceptable. Therefore, the method in this paper can be used for analysing the lift and drag characteristics of airfoils at high angle of attack comparatively.

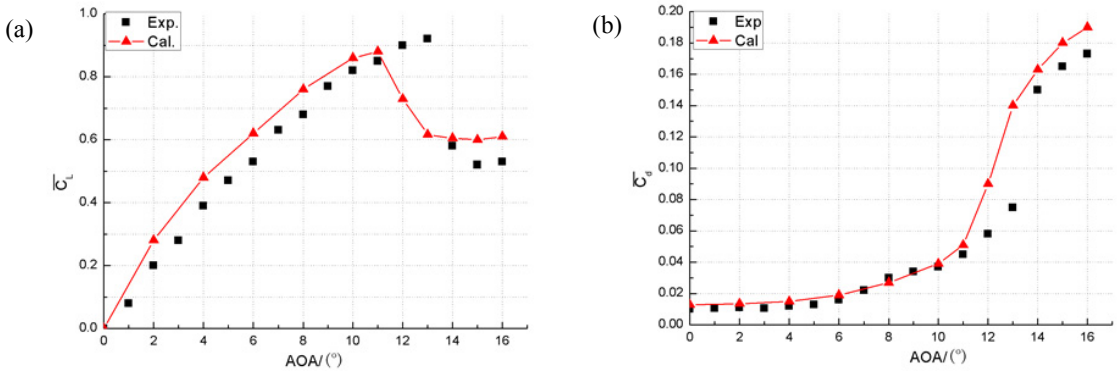

Fig. 5. Lift (a) and drag (b) coefficients curves of rigid airfoil for different angle of attack

4. Calculation results and analysis

4.1 Aerodynamic performance of segmented flexible airfoil

Table 2. Distribution forms of segmented flexible airfoils

Flexible airfoils	Flexible regions	Elastic parameter Π
Case1	[0.25,0.85]	[5.3]
Case2	[0.1,0.25,0.55]	[7.3,5.8]
Case3	[0.05,0.25,0.55,0.95]	[6.6,5.8,5.2]
Case4	[0.05,0.2,0.4,0.65,0.95]	[7.3,6.6,6.1,5.8]

It can be seen from the experimental studies for flexible membrane aircraft that the improvement on the aerodynamic performance of flexible wing at high angle of attack becomes more apparent [9]. This paper comparatively analyzed the aerodynamic parameters of different segmented forms for the flexible airfoils within the incidences range of 8°～16°. The specific parameters [16] of the four kinds of flexible airfoils are shown in Table 2. The flexible region is presented by the relative position of the chord length. The math expression of the dimensionless elastic parameter is $\Pi = (Et/qc)^{1/3}$, where E is the elastic modules, t is the thickness of the flexible membrane, q is the free stream stagnation pressure, and c is the length of the flexible segment. This parameter represents that the more flexible of the material the smaller of the Π.

The lift and drag coefficients vary with the changes of the angle of attack, which are shown in Fig 6 respectively. It can be seen from the figure that the lift coefficient for the rigid airfoil increases linearly with the increasing of the angle of attack in the case of $\alpha \leqslant 10°$, and the drag coefficient is in a lower level. And the airfoil reaches its critical

angle of attack for α =10°. When α >11°, the lift coefficient would decrease dramatically, meanwhile the drag coefficient increase rapidly.

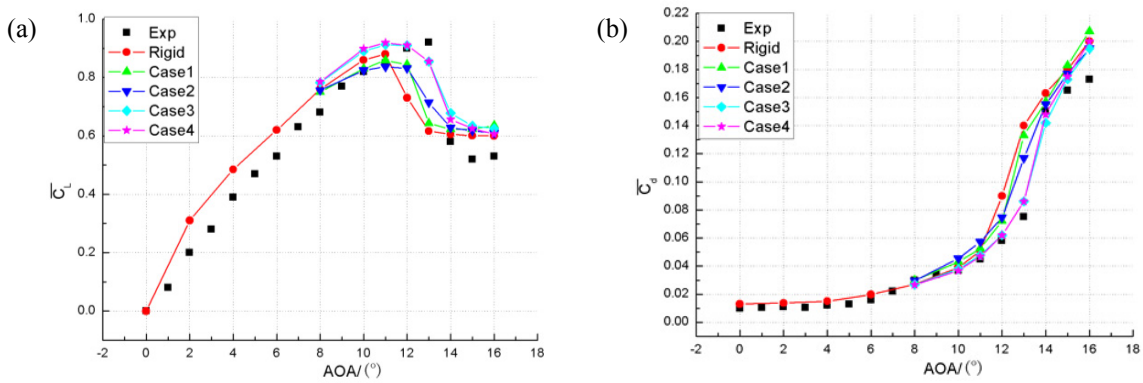

Fig. 6 Effects of segmented forms on lift (a) and drag (b) coefficients

For the four kinds of segmented flexible airfoil, when the angle of attack exceeds the critical value, their lift coefficient increases at different levels and the drag coefficient decreases similarly. Three-segment flexible airfoil performs almost the same with four-segment airfoil. The comparison of the variation trend of the maximum lift coefficient curve reveals that with the increasing number of the flexible segment, the maximum lift coefficient of the flexible airfoil increases before the stall stage, and the process entering the stall becomes slower. This phenomenon illustrates that flexibility can delay the occurrence of stall.

As for the four kinds of segmented flexible airfoils, case1 has a small elastic parameter, leading to a single oscillating law which generated by the interaction of the flexible membrane with the fluid. For this reason the lift coefficient increases slightly, and the improvement of the large scale separation on the suction side is limited at high angle of attack. Compared with case1, case2 has a larger elastic parameter relatively, a smaller flexibility, which makes it more efficient on improving its aerodynamic characteristics. While case3 could maintain a high lift coefficient and a low drag coefficient over a wide range of angle of attack. This is due to the interaction between the fluid and the multi-segment flexible membrane. The oscillating movement generates a stable region of small vortex between two adjacent flexible membranes and depresses the flow separation, which is similar to the “Fluid Roller Bearing” effect in active control. Case4 has the same flexible span with case3. Because the flexible segment connection points are clamped, the increasing segments will lead to an increase of elastic parameter and a reduction of the flexibility. So there is an optimal segmented form to gain the best aerodynamic performance improvement. In this research, the three-segment flexible airfoil could achieve the most optimal aerodynamic characteristics, and the lift coefficient increases by 39% compared with its rigid counterpart near the stall angle of attack.

4.2 Flow mechanism analysis

It is obvious in Fig 6 that the rigid airfoil has entered stall stage when the angle of attack is up to 13°, and the lift coefficients of different kinds of segmented flexible airfoils are also quite different. So analyzing the fluid flied at this angle of attack is helpful to reveal the flow mechanism.

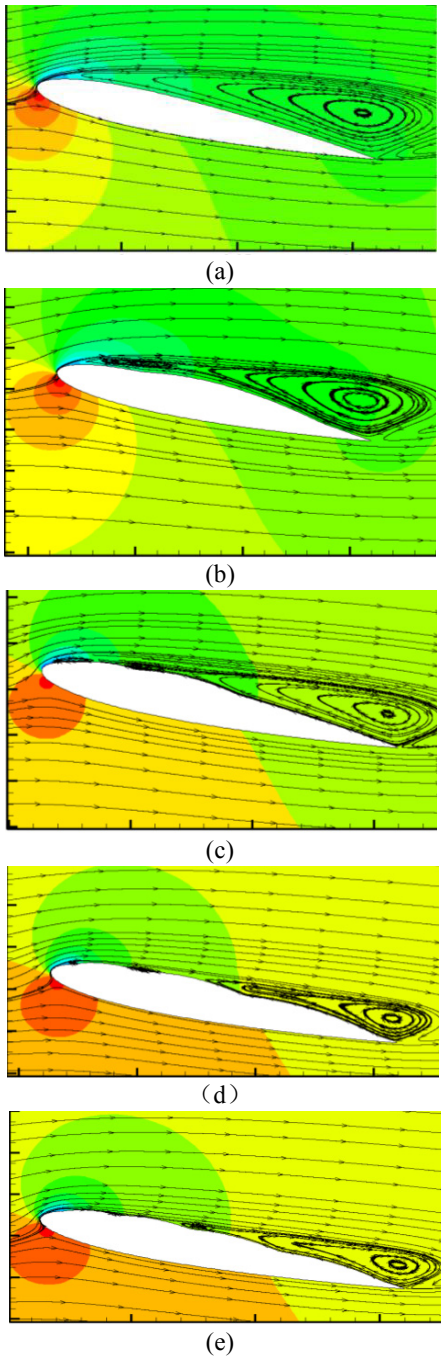

Fig. 7. Streamline of rigid and flexible airfoils（α=13°）(a), rigid; (b), one-segment; (c), two-segment; (d), three-segment; (e), four-segment

Figure 7 shows the transient flow field of rigid and four different flexible airfoils for α=13°. As can be seen from the figure, there is a large-scale flow separation on the upside of the rigid airfoil, and the airfoil is in a full stall state. The four kinds of flexible membrane could inhibit flow separation in different degrees that can be seen from

the scale of detached flow. The low pressure effect caused by the separating vortexes makes the one-segment flexible airfoil have a bulge deformation and induce an oscillating movement, which decreases the distance between the main flow and the wall as well as the scale of separating vortexes. The attached flow region becomes slightly larger in the front of the airfoil. For the two-segment flexible airfoil, the deformation and vibration become severer. One periodic small vortex begins to generate between the two segments. With the vibration of the flexible membrane, the small vortex experiences a process of producing, developing and importing into the mainstream. These small vortexes have the same direction with the mainstream, reduce the area of separation, enhance the flow orderliness, and significantly improve the lift coefficient. The small vortexes of the three and four segmented flexible airfoils are more obvious and stable. As shown in the streamline graph, the flow is almost attached to the first half-chord region, and only separates in a certain scale on the trailing edge. So the lift coefficient increases apparently, and the drag coefficient reduces effectively at the same time.

Based on the comparative analysis above, the root causes of the improvement of the flow field for the segmented flexible airfoils are small vortexes formed between the segments and the passive deformation which suppressed the separation vortex scale. These results prove that segmented flexible airfoils can optimize the aerodynamic performance and widen the range of stall angle of attack compared with the traditional rigid airfoils.

4.3 Aerodynamic load distribution

The deformation and oscillating movement of the flexible membrane interact with the detached vortexes from the upper surface. This interaction affects the flow field mainly in the first half chord region. Aerodynamic loads on the airfoil have great diversity along the chord direction. Figure 8 shows the time-average pressure coefficient distribution for rigid and flexible airfoils at 13° and 14° angles of attack respectively.

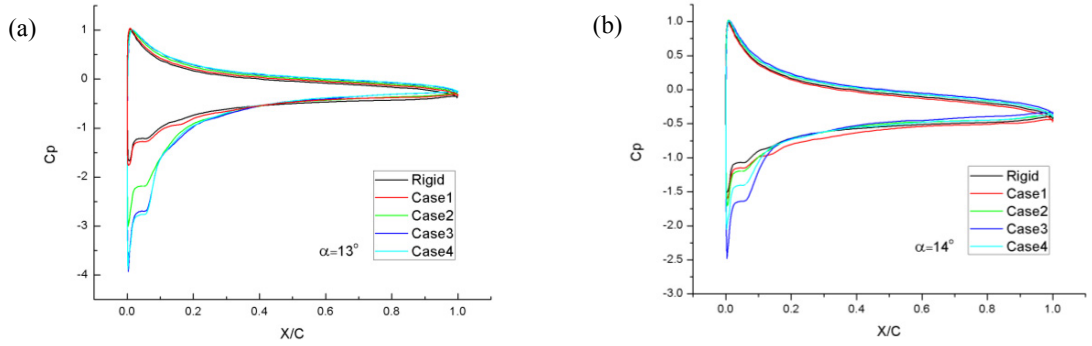

Fig. 8. Distribution of pressure coefficients of rigid and flexible airfoils of 13°(a) and 14°(b) angle of attack

The pressure coefficient curves illustrate that the segment forms have significant impact on the pressure distribution near the leading edge. At 13° angle of attack, large scale separation appears in the front of the rigid airfoil, so the pressure coefficient on the upper surface is in a higher level, and the pressure difference between the two sides of the airfoil is smaller, which leads to a low lift coefficient relatively. There is a small local deformation and vibration on the one-segment flexible airfoil, but its ability of improving the flow field is limited, which makes it similar to the rigid airfoil. Two-segment flexible airfoil has a better performance. The combination of deformation and vibration between the different segments is helpful to maintain the small interval vortexes, decrease the pressure coefficient in the front of the airfoil and extend the influencing area to the middle of the chord. The three and four segmented flexible airfoils have a similar distribution trend of the pressure coefficient. It also indicates that they share the analogous feature on improving the aerodynamic performance. When the angle of attack reaches 14°, the pressure coefficients of the segmented flexible airfoils rebounds sharply in the front area of the upper surface and the pressure difference on both sides of the airfoil reduces, which makes a dramatic drop on lift coefficient. The pressure difference of the four kinks of segmented flexible airfoils decreases gradually. Three-segment flexible airfoil has the lowest static pressure coefficient on the upper surface among the four airfoils, corresponding with the

best lift coefficient, which is shown in Fig 6. Consequently, there is a proper distribution form of the segmented flexible airfoil to achieve the best improvement of the flow field. In this paper, three-segment form has the most optimal aerodynamic characteristics and could be used for aircrafts, turbo machineries and other related devices in the future.

5. Conclusions

In the present work, fluid-structure interaction technology was used to investigate the aerodynamic characteristics and flow field for the rigid and segmented flexible airfoils based on NACA0012. The transition process and structural response were considered in this simulation. Based on the analysis of aerodynamic parameters and flow details caused by the segmented forms and flexible deformation, several important conclusions are concluded as follows:

- The airfoils with the segmented flexible structure on the upper surface have a higher stall angle of attack and provide a better lift coefficient, which can delay the stall effectively.
- The flow mechanism of the segmented flexible airfoil on improving the lift performance at high angles of attack is that deformation of the flexible membrane suppresses the scale of the separated flow and small interval vortexes generated between the segments are stably existed. These small vortexes have the same effect which called “Fluid Roller Bearing” and impel the flow attach to the airfoil surface.
- Among the four kinds of segmented forms, three-segment flexible airfoil has the best aerodynamic characteristics, which create a profit of 39% on lift coefficient compared with the traditional rigid airfoil.

Acknowledgements

The authors would like to acknowledge funding from the National Natural Science Foundation of China (No. 51106003). We also appreciate the useful communication with colleagues in the National Key Laboratory on Aero-Engines.

References

[1]Gabor O S, Koreanschi A, Botez R M. Low-speed aerodynamic characteristics improvement of ATR 42 airfoil using a morphing wing approach. [C]. IECON 2012-38th Annual Conference on IEEE Industrial Electronics Society. IEEE, 2012: 5451-5456.

[2] CHEN Qian, BAI Peng, YING Wei long, LENG Jing song, AHAN Hui ling, LIU Zi qiang. Analysis on the aerodynamic characteristics of variable camber airfoils with continuous smooth morphing trailing edge. [J]. ACTA AERODYNAMICA SINICA, 2010, 1(28).

[3] Chui jie W, Yan qiong X, Jie zhi W. “Fluid roller bearing” effect and flow control. [J]. Acta Mechanica Sinica, 2003, 19(5): 476-484.

[4]GUO Qiu ting, ZHANG Lai ping, CHANG Xin hua, HE Xin. Numerical simulation of unsteady turbulence flow over multi-element airfoil with local active morphing for separation flow controlling. [J].ACTA AERODYNAMIC SINICA, 2011, 29(5): 607-612.

[5]Curet O M, Carrere A, Waldman R, et al. Aerodynamic Characterization of Wing Membrane with Adaptive Compliance. [J]. 2013.

[6]Lian Y, Shyy W, Viieru D, et al. Membrane wing aerodynamics for micro air vehicles. [J]. Progress in Aerospace Sciences, 2003, 39(6): 425-465.

[7]Lian Y, Shyy W. Three-dimensional fluid-structure interactions of a membrane wing for micro air vehicle applications. [J]. AIAA Paper, 2003, 1726.

[8]Gordnier R E. High fidelity computational simulation of a membrane wing airfoil. [J]. Journal of Fluids and Structures, 2009, 25(5): 897-917.

[9]Albertani R, Stanford B, Hubner J P, et al. Aerodynamic coefficients and deformation measurements on flexible micro air vehicle wings. [J]. Experimental Mechanics, 2007, 47(5): 625-635.

[10]Hu H, Tamai M, Murphy J T. Flexible-membrane airfoils at low Reynolds numbers. [J]. Journal of Aircraft, 2008, 45(5): 1767-1778.

[11]Rojratsirikul P, Wang Z, Gursul I. Unsteady fluid–structure interactions of membrane airfoils at low Reynolds numbers. [J]. Experiments in Fluids, 2009, 46(5): 859-872.

[12]Shyy W, Klevebring F, Nilsson M, et al. Rigid and flexible low Reynolds number airfoils. [J]. Journal of Aircraft, 1999, 36(3): 523-529.

[13] Castelli M R, Garbo F, Benini E. Numerical investigation of laminar to turbulent boundary layer transition on a Naca 0012 airfoil for vertical-axis wind turbine applications. [J]. Wind Engineering, 2011, 35(6): 661-686.

[14] Menter F R, Langtry R B, Likki S R, et al. A correlation-based transition model using local variables: Part I—model formulation. [C]. Vienna. Austria. ASME Turbo Expo 2004: Power for Land, Sea, and Air. American Society of Mechanical Engineers, 2004: 57-67.

[15] Lee T, Gerontakos P. Investigation of flow over an oscillating airfoil. [J]. Journal of Fluid Mechanics, 2004, 512: 313-341.

[16] Smith R, Shyy W. Computation of aerodynamic coefficients for a flexible membrane airfoil in turbulent flow: a comparison with classical theory. [J]. Physics of Fluids (1994-present), 1996, 8(12): 3346-3353